Journal Pre-proofs

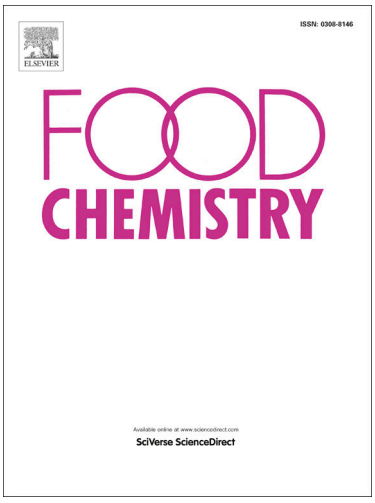

Well-orientation strategy for direct binding of antibodies: Development of the immunosensor using the antigen modified Fe_2O_3 nanoprobes for sensitive detection of aflatoxin B_1

Kunyi He, Tong Bu, Shuang Zhao, Feier Bai, Meng Zhang, Yongming Tian, Xinyu Sun, Mengna Dong, Li Wang

PII: S0308-8146(21)00589-6
DOI: https://doi.org/10.1016/j.foodchem.2021.129583
Reference: FOCH 129583

To appear in: *Food Chemistry*

Received Date: 6 November 2020
Revised Date: 24 December 2020
Accepted Date: 7 March 2021

Please cite this article as: He, K., Bu, T., Zhao, S., Bai, F., Zhang, M., Tian, Y., Sun, X., Dong, M., Wang, L., Well-orientation strategy for direct binding of antibodies: Development of the immunosensor using the antigen modified Fe_2O_3 nanoprobes for sensitive detection of aflatoxin B_1, *Food Chemistry* (2021), doi: https://doi.org/10.1016/j.foodchem.2021.129583

Well-orientation strategy for direct binding of antibodies: Development of the immunosensor using the antigen modified Fe_2O_3 nanoprobes for sensitive detection of aflatoxin B_1

Kunyi He,[†,#] Tong Bu,[†,#] Shuang Zhao,[†] Feier Bai,[†] Meng Zhang,[†] Yongming Tian,[†] Xinyu Sun,[†] Mengna Dong,[†] and Li Wang[†*]

[†] College of Food Science and Engineering, Northwest A&F University, Yangling 712100, Shaanxi, China

[*] Author for correspondence:

Tel.: +86 29-8709-2486

Fax: +86 29-8709-2486

lwang@nwsuaf.edu.cn

[#] These authors contributed equally to this work.

ABSTRACT

Sensitive immunochromatography test strip (ICTS) is a crucial and convenient method

in point-of-care testing for food safety. However, traditional ICTSs are accustomed to labeling monoclonal antibodies (mAbs) on the nanomaterials (NMs-mAb) as probes, which were restricted by the number and direction of mAbs or complicated chemical coupling reactions between mAbs and nanomaterials. Herein, we proposed a novel ICTS based on Fe_2O_3 nanostructures (FNSs) coupled with antigens (FNS-ag) as signal tags to conjugate mAbs directionally (FNS-ag-DICTS) for aflatoxin B_1 (AFB_1) detection. The prepared FNS-ag can improve the binding efficiency of mAbs and enhance the detection sensitivity, waiving the intrinsic limitations of NMs-mAb. Under the optimal experimental conditions, FNS-ag-DICTS possessed excellent specificity and a wide detection range, with a visual detection limit (vLOD) of 0.0125 ng mL^{-1}. In addition, the biosensor successfully detected AFB_1 in peanut, green bean and corn, with an average recovery rate of 82.8-124.9%.

Keywords: Immunochromatography test strips; Fe_2O_3 nanostructure; Orientated connection; Aflatoxins B_1; Wide detection range

1. Introduction

Aflatoxin B_1 (AFB_1), a bifuran ring toxoid that commonly found in grains, oils and their products, is produced mainly by strains such as Aspergillus flavus and Aspergillus parasiticus.(Haque et al., 2020; Rushing & Selim, 2019) AFB_1 possesses high toxicity, mutagenicity and carcinogenicity, and it is difficult to degrade, causing AFB_1 to pose a danger to humans and animals.(Al-Jaal, Jaganjac, Barcaru, Horvatovich, & Latiff, 2019; Rushing et al., 2019; Wang, Yang, & Wu, 2020) Due to increasing concerns over food

safety and health, it is urgent to establish a sensitive, specific, rapid and convenient technology for AFB_1 detection.

Currently, a variety of methods such as high-performance liquid chromatography (HPLC),(Chen, Luan, Wang, Wang, & Shao, 2017; Choochuay, Phakam, Jala, Maneeboon, & Tansakul, 2018) surface enhanced Raman scattering (SERS),(Gillibert, Huang, Zhang, Fu, & Lamy de la Chapelle, 2018; Li et al., 2018) electrochemical detection, liquid chromatography tandem mass spectrometry (LC-MS/MS),(Flores-Flores & Gonzalez-Penas, 2017; Schlegel & Elsinghorst, 2020) fluorescence detection and enzyme linked immunosorbent assay (ELISA)(Jia et al., 2020; Oplatowska-Stachowiak et al., 2016; Z. Xu, Long, Chen, Chen, & Cheng, 2021) testing have been developed to detect AFB_1. However, these techniques show a lack of balance with time consumption, expediency and simple measurements, causing a restriction under on-site conditions.(Blazkova, Javurkova, Fukal, & Rauch, 2011; Singh, Huang, Wang, Shao, & Zhang, 2020) Immunochromatography test strip (ICTS), as a low-cost, apparatus-free and fast detection platform, is a promising strategy that satisfy the point-of-care testing (POCT).(Aoyama, Monden, Akiyama, Yamada, & Seki, 2019; Guo et al., 2019; S. Xu et al., 2019)

It is worth noting that the sensitivity of ICTS is greatly affected by the method and efficiency of coupling monoclonal antibodies (mAbs) to nanomaterials, as well as the amounts of Fab regions of mAbs exposed to antigen binding.(Di Nardo, Cavalera, Baggiani, Giovannoli, & Anfossi, 2019; Liu et al., 2020; Yao et al., 2019) In general, mAbs were directly labeled with various nanomaterials through electrostatic adsorption

or covalent coupling to obtain probes.(Akram et al., 2020; S. Xu et al., 2019) However, in the electrostatic adsorption method, the binding method is easily affected by mAbs isoelectric point, temperature, pH, and other factors, resulting in a decrease in selective binding ability of mAbs.(Di Nardo et al., 2019; Jeong et al., 2017; Lou et al., 2018) In covalent coupling method, the conjugation efficiency and activity of mAbs may be weakened by covalent bonds randomly occupying active primary amine functional groups of mAbs, which inevitably blocks a part of the antigen binding sites on the mAbs.(Di Nardo et al., 2019; Jeong et al., 2017) In addition, the above methods all make the orientation of the mAbs on the nanomaterials surface random, rendering the Fab region partially or completely losing its access to antigens. Compared with mAbs immobilized on the surface of nanomaterials, free specific mAbs feature higher biological activity, faster Brownian motion and more opportunities to bind to the analyte in the sample solution.(Yao et al., 2019) Hence, a new strategy for directional conjugation of mAbs under a simple process is essentially needed to fulfill the demands for highly sensitive measurements.

In this study, a novel competitive ICTS strategy in which Fe_2O_3 nanostructures (FNSs) bound antigens to form FNS-ag probes and then directionally connected mAbs was developed (FNS-ag-DICTS), which was used for ultrasensitive, specific, rapid and cost-effective detection of AFB_1. The new FNSs synthesized by one-step hydrothermal method was more suitable for labeling antigens by general electrostatic adsorption due to its high porosity, large surface area, excellent optical property, and chemical stability.(Gurav et al., 2020; Lin et al., 2017) The merit of this strategy was that FNS-

ag probes could combine the Fab region of the free mAbs and reduce the amount of mAbs used. Due to the significant reduction in the amount of free mAbs, when AFB_1 was present in the sample solution, the competition between free AFB_1 and AFB_1-BSA became more intense, thereby amplifying the detection signal and helping to improve the sensitivity of the assay.(Butler, Pearce, Nail, Vincent, & Sava Gallis, 2020; Jeong et al., 2017; Yao et al., 2019) Under the optimal conditions, the FNS-ag-DICTS showed a low detection limit, wide detection range and excellent selectivity to AFB_1. Moreover, the feasibility and applicability of FNS-ag-DICTS were further evaluated by testing AFB_1 in peanut, green bean and corn samples. In summary, the novel method based on FNS-labeled antigen-directed connection of mAbs has an excellent application value as a simple, fast and efficient biosensor in food safety detection.

2. Materials and methods

2.1 Materials.

Iron chloride hexahydrate ($FeCl_3 \cdot 6H_2O$) was obtained from Guangdong Guanghua Sci-Tech Co., Ltd. (Guangdong, China). N, N'-dimethylformamide (DMF), benzoic acid and methanol were purchased from Chengdu Kelong Chemical Co., Ltd. (Chengdu, China). Bovine serum albumin (BSA) was provided by DIYI Biotechnology Co., Ltd. (Shanghai, China). Goat anti-mouse immunoglobulin (IgG) and anti-AFB_1 monoclonal antibodies (anti-AFB_1-mAbs) were purchased from Wuhan Amyjet Scientific Co., Ltd. (Wuhan, China). Aflatoxin B_1 (AFB_1), aflatoxin B_2 (AFB_2), aflatoxin G1 (AFG_1), deoxynivalenol (DON), fumonisin B_1 (FB_1), ochratoxin A (OTA), patulin (PAT) and zearalenone (ZEA) (Their chemical structures were shown in Fig. S1) were all offered

from Beijing Prime Bio Tek Technology Co., Ltd. (Beijing, China). Nitrocellulose (NC) membrane, glass fiber membrane, polyvinyl chloride plate and absorbent pad were obtained from Shanghai Dening Technology Co., Ltd. (Shanghai, China). Ultrapure water comes from the Millipore Milli-Q purification system in our laboratory. Peanut, green bean and corn samples were all bought from a local supermarket (Yangling, China). All solvents and other chemical reagents used in this experiment were of analytical grade.

2.2 FNSs preparation.

The FNSs consist of $FeCl_3 \cdot 6H_2O$ (99%), benzoic acid (97%) and DMF (99%) with a molar ratio of 1: 1: 380. After stirring for 15 minutes, the above solution was mixed in a steel autoclave lined with Teflon, and further heated at 160 °C for 72 hours. After the solution was cooled down to room temperature, the resulting sediment was collected by centrifugation and washed with DMF 3 times. Ultimately, the synthetic granule product was placed under vacuum and desiccated at 60 °C overnight, and stored in a drying cabinet for further use.

2.3 Construction of the directional FNS-ag probes.

Applying a different coupling reaction from the past, directional FNS-antigen (FNS-ag) probes were synthesized innovatively. In short, 1 μg of AFB_1-BSA was added to 1 mL of prepared FNSs solution, and then violently mixed for 40 min at room temperature. The residual binding sites on the surface of FNSs were blocked with 10% BSA solution. The mixture was incubated for 50 min, and the excess reagents were discarded after centrifugation (10,000 rpm, 10 min). Finally, the obtained FNS-ag probes were

resuspended in 20 μL of ultrapure water and stored at 4 °C to conserve biological activity for further use.

2.4 Fabrication of the FNS-ag-DICTS.

In the fabrication of FNS-ag-DICTS, the polyvinyl chloride plate served as the support, onto which the sample pad, conjugate pad, NC membrane and absorption pad were laminated at an overlapping position of 1-3mm. The sample and conjugate pads were blocked by immersing in 10 mM phosphate buffered saline (PBS) containing 2% BSA, and then dried at 37 °C for 8 h. The test line (T-line) of the NC membrane was painted in IgG (0.5 mg mL^{-1}) at a speed of 0.8 μL cm^{-1}, then the NC membrane was stored at room temperature for drying overnight.(T. Bu et al., 2020; Bu et al., 2019) Finally, all the components were pasted on the plate successively, cut into 3 mm wide strips and stored at 4 °C for further use.

2.5 Immunoassay program and performance assessment of FNS-ag-DICTS.

In order to analyze the peculiarity of this FNS-ag-DICTS under best conditions, different concentrations of AFB_1 were dissolved in the 0.01 M PBS solution to acquire the test samples (0, 0.0064, 0.0125, 0.025, 0.05, 0.1, 0.2, 0.4, 0.8, 1.6, 3.2, 6.4, 12.8, 25.6 ng mL^{-1}). Firstly, 0.4 μL mAbs (0.1 mg mL^{-1}) was incubated with 100 μL test sample solution at room temperature for 20 min, then FNS-ag probes (2.0 μL) were added and mixed. After immersing the sample pad in the above compound for 15 minutes, the results were recorded by a camera and the T-line signal values were read by a strip reader.

The specificity of the strip was verified by testing AFB_1 (12 ng mL^{-1}) and other

mycotoxins including AFB_2, AFG_1, DON, FB_1 OTA, PAT and ZEA (100 ng mL^{-1}).

2.6 Detection of AFB_1 in spiked real samples.

Peanut, green bean and corn were used as real samples in this experiment. The homogeneous foodstuffs (2 g) were triturated, blended severely with 4 mL methanol-PBS (70:30, v/v) for 20 min, and extracted with ultrasonic for 10 min, respectively.(Bu et al., 2019) Then the insoluble matter was removed through centrifugation at 8000 rpm for 10 min. And the obtained supernatant was diluted 40-folds with 10mM PBS (0.01 M, pH 7.0). The spiked real samples were analyzed via the prepared FNS-ag-DICTS on the basis of section 2.5.

3. Results and discussions

3.1 Principle of the FNS-ag probes on the emulative FNS-ag-DICTS.

Different from the traditional nanomaterials labeled mAbs as probe, in this paper, the FNSs with excellent water-dispersibility and stability were prepared by one-step hydrothermal method, they could label AFB_1-BSA on their surfaces to form FNS-ag probes (Scheme 1A). For competitive immunoassays, AFB_1-BSA and AFB_1 compete to bind Fab regions of mAbs. In the traditional ICTS, the random combination of nanomaterials and mAbs made some Fab regions of the mAbs blocked, resulting in mAbs unable to effectively participate in the competitive immune response, which greatly limited the sensitivity of detection and wasted mAbs. In the FNS-ag-DICTS strategy, the AFB_1-BSA was preferentially immobilized on the surfaces of the FNSs, the specific binding sites of the Fab regions were not masked because the mAbs were free, which could efficiently bind AFB_1 or FNS-ag probes (Scheme 1B).

In the detection process, the sample solution was mixed with anti-AFB_1 mAbs and incubated for a period of time to make them fully bound, then added the FNS-ag probes to bind the remaining unbound mAbs. The mixture was added to the sample pad, migrated along the sample pad to the absorption pad under the capillary action. If there were no AFB_1 molecules in the sample solution, the FNS-ag-mAb was combined with the immobilized goat anti-mouse IgG and a visible signal was discovered on T-line. When AFB_1 existed in the sample, the limited mAbs would bind to AFB_1 firstly, and the remaining mAbs would combine to the FNS-ag probes, so the signal on the T-line would be weaker than the blank. In this measurement mode, the intensity of the color signal was inversely proportional to the concentration of the target in the actual samples. When the target concentration was high enough, no obvious band can be seen on the T-line (Scheme 1C). In short, the use of FNS-ag probes that were oriented to connect mAbs effectively reduced the amounts of mAbs, exposed the Fab binding regions of mAbs, and obtained a wide detection range.

3.2 Characterizations of the FNSs and the FNS-ag probes.

As mentioned above, the as-synthesized FNSs were utilized to label AFB_1-BSA as the signal-generation tags in the ICTS. Scanning electron microscopy (SEM) image showed that the prepared FNSs had a cubic shape and were relatively uniformly distributed (Fig. 1A), with an average particle size of 79.53 nm (Fig. 1B). The X-ray diffraction (XRD) pattern of the prepared FNSs matched well with that of standard pattern No.33-0664 in the JCPDS card, proving the formation of Fe_2O_3 (Fig. 1C).(Radu, Iacovita, Benea, & Turcu, 2017) To confirm the successful preparation of FNSs, X-ray

photoelectron spectroscopy (XPS) was used for analysis. Fig. 1D indicated that the synthesized FNSs mainly composed of three elements Fe, O and C. The two peaks worthy of consideration were located at around 710 eV and 724 eV, which belong to Fe $2p_{1/2}$ and Fe $2p_{3/2}$, respectively. 719 eV and 733 eV were the satellite peaks of Fe^{3+}, which were exactly the same as the characteristic peaks of Fe_2O_3 nanoparticles (Fig. 1E).(Abhilash, Gangadhar, Krishnegowda, Chikkamadaiah, & Srikantaswamy, 2019; Gurav et al., 2020; Pauly, Yubero, Espinós, & Tougaard, 2019) Further analysis of the fitted O 1s spectrum (Figure 1F) showed that the main O 1s peak occurred at 530.25 eV, which was ascribed to Ox^{2-}, confirmed the presence of Fe_2O_3 compound. The subpeaks at 531.5 eV and 532.8 eV were commonly attributed to OH^- and O_2^{2-} / O^-, respectively.(Kaspar et al., 2019)

Moreover, UV-vis spectroscopy confirmed that FNSs can bind to protein (Fig. 1G). The characteristic absorption peak of BSA was observed in the FNS-BSA at 280 nm, indicating that the protein was successfully labeled on the surface of FNSs. Fourier transform infrared (FT-IR) spectroscopy was scanned to ascertain the composition of FNSs. The characteristic absorption signals of Fe-O bond appeared around at 565 cm^{-1}, and the signals at near 3466 cm^{-1} and 1634 cm^{-1} were identified as -OH and C=O stretching vibration and bending vibration, respectively.(Jana et al., 2017; Ouyang, Zhao, Suib, & Yang, 2019; Zhou et al., 2018) In addition, the FT-IR spectrum of FNS-BSA had the same characteristic absorption peaks as those of FNSs and BSA (Fig. 1H), indicating that protein was indeed connected to FNSs.(Cheng et al., 2019) To further evaluate that FNSs can label protein, sodium dodecyl sulfate-polyacrylamide gel

electrophoresis (SDS-PAGE) was used for analysis. In Fig. 1I, there was no band when only FNSs were presented, while both of BSA and FNS-BSA had blue bands at a molecular weight of about 60 kDa, which proved that FNSs can couple protein well.(Bu et al., 2020)

3.3 Optimization of FNS-ag-DICTS conditions.

In this work, the signal intensity on the T-lines (FI_T) for the AFB_1-free sample and the competitive inhibition rate for the AFB_1-spiked sample (12.8 ng mL^{-1}) were adopted to select the optimal detection parameters. The competitive inhibition rate was calculated by $(1\text{-}B/B_0) \times 100\%$, where B_0 and B were FI_T values of AFB_1-free and AFB_1-spiked solutions, respectively. Firstly, opportune concentration of immobilized AFB_1-BSA was the pivotal condition to achieve best performance. The signal intensity on T-line augmented as the AFB_1-BSA concentration increased from 2.5 to 20 μg mL^{-1}, but the maximum inhibition rate of 78% was acquired when AFB_1-BSA concentration reached 10 μg mL^{-1} (Fig. 2A). So, 10 μg mL^{-1} of AFB_1-BSA was deemed to the optimum supplemental levels in the FNSs solution. Moreover, the concentration of IgG (0.25, 0.5, 0.75, and 1 mg mL^{-1}) on T-line were studied. In Fig. 2B, the T-line intensity increased as the IgG concentration increased, and when the concentration of IgG was 0.5 mg mL^{-1}, the highest inhibition rate of 79% was obtained. Therefore, in FNS-ag-DICTS, IgG of 0.5 mg mL^{-1} was selected as the best concentration. In Fig. 2C, the signal intensity on T-line was gradually increased when the volume of FNS-ag probe changed from 0.5 to 2.5 μL. However, excessive amounts of probes would lead to a reduction in inhibition rate and low sensitivity, which was not conducive to detection.

Taking into account the factors such as signal strength, inhibition rate, and measurement sensitivity, 2 μL was used as the optimal volume of FNS-ag probe. For competitive immunoassay, reducing the use of mAbs usually lead to a low detection limit, and can effectively increase the inhibition rate. In Fig. 2D, as the amount of mAbs increased, the signal intensity on the T-line enhanced. 0.4 μg mL^{-1} mAbs was chosen as the optimal usage amount because the detection system achieved a maximum inhibition rate of 80%. Compared with the traditional FNS-mAb-ICTS, the mAbs dosage of FNS-ag-DICTS had been reduced from 10 μg mL^{-1} to 0.4 μg mL^{-1}, which greatly improved the detection performance. As a key factor affecting the efficiency of the competition between AFB_1 and FNS-ag probes, the incubation time of AFB_1 and mAbs were optimized. In Fig. 2E, 20 min was selected as the best incubation time. Furthermore, when the immunoreaction time was increased from 0 to 15 min, the inhibition rate was enhanced from 69% to 80% (Fig. 2F). Thereby, 15 min was regarded as the optimal immunoreaction time. In addition, in order to further improve the analysis capability, the influence of BSA closure time and pH environment on the detection performance were also optimized. The maximum inhibition rate proved that the optimal incubation time was 50 min and the optimal reaction pH was 7 (Fig. S2A and S2B).

3.4 Analytical performance of FNS-ag-DICTS.

Sensitivity is an essential parameter to evaluate the performance of FNS-ag-DICTS. Under the optimized conditions, a series of concentrations of AFB_1 standard solutions were tested to evaluate the sensitivity and dynamic range of the proposed platform. The

result in Fig. 3A showed that with the increased of AFB_1 in the test solution, the color intensity of the T-line decreased. In addition, when the concentration of AFB_1 was 0.0064 ng mL^{-1}, the T-line intensity was the same as that of the negative control strip, and the minimum AFB_1 concentration of 0.0125 ng mL^{-1} could make the color intensity differ from that of the negative control strip. Here, 0.0125 ng mL^{-1} could be regarded as the visual detection limit (vLOD) (The vLOD is defined as the lowest concentration of the target whose observed T-line color is weaker than that of the blank) of the FNS-ag-DICTS.

In this study, the standard curve of the FNS-ag-DICTS for AFB_1 quantitative determination was indicated by drawing the intensity value of T-line vs the logarithm of AFB_1 concentrations (0-25.6 ng mL^{-1}). The standard curve exhibited a good linear relationship in the detection range of AFB_1 from 0 to 12.8 ng mL^{-1}, the correlation coefficient R^2=0.994, the IC_{50} value of FNS-ag-DICTS was 0.30 ng mL^{-1}, and the regression equation could be expressed as Y= -226.44X+346.48, where X and Y were represented Lg [AFB_1 concentration] and T-line intensity, respectively (Fig. 3B).

The traditional FNS-mAb-ICTS was prepared to confirm the improvement of sensor sensitivity. The best experimental conditions and linear relationships were shown in the supporting information. As shown in Fig. S4, the vLOD of AFB_1 detected by traditional FNS-mAb-ICTS was 0.09 ng mL^{-1}. Thus, the sensitivity of the developed FNS-ag-DICTS using FNS-ag as a probe was at least seven times higher than that of traditional FNS-mAb-ICTS. This fact may be because the mAbs in FNS-ag-DICTS were oriented to bind to FNS-ag, thereby reducing the amount of mAbs used and

increasing the sensitivity.(Tong Bu et al., 2020; Liu et al., 2020; Yao et al., 2019) In addition, the vLOD of FNS-ag-DICTS was lower than most previous reports on the detection of AFB_1 (Table S1).

The selectivity of the FNS-ag-DICTS sensor was evaluated by analyzing two common structural analogues AFG_1 and AFB_2 (100 ng mL^{-1}) and five other common mycotoxins (DON, FB_1, OTA, PAT, ZEA) (100 ng mL^{-1}). The results in Fig. 3C and 3D indicated that the developed FNS-ag-DICTS only exhibited a lighter T-line color in the presence of AFG_1 and AFB_2, while the T-line intensities of other mycotoxins were basically the same as the negative control strip. In order to further confirm the specificity of FNS-ag-DICTS, the same anti-AFB_1 mAbs were also used to detect 12.8 ng mL^{-1} of AFB_1 and 100 ng mL^{-1} of other toxins by competitive ELISA (Fig. S5). The results indicated that except for AFG_1 and AFB_2 (less than 0.1), the values of other toxins were the same as the control (about equal to 1). The above results demonstrated that the prepared FNS-ag-DICTS had high specificity for the detection of AFB_1.

3.5 AFB_1 analysis in actual samples.

In order to further prove the feasibility of the FNS-ag-DICTS in the application of food samples, the peanut, green bean and corn samples were first processed according to the previous method, and then the acquired sample solutions were detected by the FNS-ag-DICTS. As shown in Fig. 4, as the concentration of AFB_1 increased, the T-line intensity gradually decreased. At the same time, the vLODs of AFB_1 in the three spiked samples were all 0.0125 ng mL^{-1}. In addition, the results in Table 1 showed that the average recovery rate of AFB_1 was 82.8-124.9%, and the relative standard deviation

(RSD) values was lower than 5.9%. The above results showed that the developed FNS-ag-DICTS could be used for AFB_1 detection in complex foods after simple pretreatment, and possessed good application potential and reproducibility.

4. Conclusion

In conclusion, we successfully developed the FNS-ag-DICTS to detect AFB_1 sensitively. Since the free mAbs had higher biological activity and affinity for the target analyte, the FNS-labeled antigen was used to prepare FNS-ag probes to directionally connect the free mAbs, and the detection sensitivity could be improved by using fewer mAbs. Under optimal conditions, the detection limit of the designed FNS-ag-DICTS was 0.0125 ng mL^{-1}, which was 7 times lower than the detection limit of traditional FNS-ICTS based on the FNS-mAb probe and had a wider detection range. In addition, the new FNS-ag-DICTS sensor had a wide detection range and enabled rapid screening of AFB_1 in peanut, green bean and corn samples. Overall, this novel FNS-ag-DICTS with directionally linked mAbs had the advantages of rapidity, sensitivity, low cost and portability, and was worthy of being widely used in food safety testing.

Declaration of interests

The authors declare no competing financial interest.

Acknowledgments

This work was supported by Talented Program (A279021724) and the Fundamental Research Funds for the Northwest A&F University (Nos. Z111021601).

References

Abhilash, M. R., Gangadhar, A., Krishnegowda, J., Chikkamadaiah, M., &

Srikantaswamy, S. (2019). Hydrothermal synthesis, characterization and enhanced photocatalytic activity and toxicity studies of a rhombohedral Fe_2O_3 nanomaterial. *RSC Advances, 9*(43), 25158-25169. https://doi.org/10.1039/c9ra04978a.

Akram, A., khan, A., Majdinasab, M., Abbas, G., Raza, R., Ahmad, M. A., & Hayat, A. (2020). Development of a fluorescence immunoassay based on X-Ti-Zn nanocomposite for the detection of MUC1 biomarker. *Sensors and Actuators B: Chemical, 320*(2020), 128413. https://doi.org/10.1016/j.snb.2020.128413.

Al-Jaal, B. A., Jaganjac, M., Barcaru, A., Horvatovich, P., & Latiff, A. (2019). Aflatoxin, fumonisin, ochratoxin, zearalenone and deoxynivalenol biomarkers in human biological fluids: A systematic literature review, 2001-2018. *Food Chem Toxicol, 129*, 211-228. https://doi.org/10.1016/j.fct.2019.04.047.

Aoyama, S., Monden, K., Akiyama, Y., Yamada, M., & Seki, M. (2019). Enhanced Immunoadsorption on Imprinted Polymeric Microstructures with Nanoengineered Surface Topography for Lateral Flow Immunoassay Systems. *Anal Chem, 91*(21), 13377-13382. https://doi.org/10.1021/acs.analchem.9b03454.

Blazkova, M., Javurkova, B., Fukal, L., & Rauch, P. (2011). Immunochromatographic strip test for detection of genus Cronobacter. *Biosens Bioelectron, 26*(6), 2828-2834.

https://doi.org/10.1016/j.bios.2010.10.001.

Bu, T., Jia, P., Sun, X., Liu, Y., Wang, Q., & Wang, L. (2020). Hierarchical molybdenum disulfide nanosheets based lateral flow immunoassay for highly sensitive detection of tetracycline in food samples. *Sensors and Actuators B: Chemical, 320*(2020), 128440. https://doi.org/10.1016/j.snb.2020.128440.

Bu, T., Yao, X., Huang, L., Dou, L., Zhao, B., Yang, B., . . . Zhang, D. (2020). Dual recognition strategy and magnetic enrichment based lateral flow assay toward Salmonella enteritidis detection. *Talanta, 206*, 120204. https://doi.org/10.1016/j.talanta.2019.120204.

Bu, T., Zhang, M., Sun, X., Tian, Y., Bai, F., Jia, P., . . . Wang, L. (2019). Gold nanoparticles-functionalized microorganisms assisted construction of immunobiosensor for sensitive detection of ochratoxin A in food samples. *Sensors and Actuators B: Chemical, 299*(2019), 126969. https://doi.org/10.1016/j.snb.2019.126969.

Butler, K. S., Pearce, C. J., Nail, E. A., Vincent, G. A., & Sava Gallis, D. F. (2020). Antibody Targeted Metal-Organic Frameworks for Bioimaging Applications. *ACS Appl Mater Interfaces, 12*(28), 31217-31224. https://doi.org/10.1021/acsami.0c07835.

Chen, F., Luan, C., Wang, L., Wang, S., & Shao, L. (2017). Simultaneous determination of six mycotoxins in peanut by high-performance liquid chromatography with a fluorescence detector. *J Sci Food*

Agric, 97(6), 1805-1810. https://doi.org/10.1002/jsfa.7978.

Cheng, N., Shi, Q., Zhu, C., Li, S., Lin, Y., & Du, D. (2019). Pt-Ni(OH)2 nanosheets amplified two-way lateral flow immunoassays with smartphone readout for quantification of pesticides. *Biosens Bioelectron, 142*, 111498. https://doi.org/10.1016/j.bios.2019.111498.

Choochuay, S., Phakam, J., Jala, P., Maneeboon, T., & Tansakul, N. (2018). Determination of Aflatoxin B_1 in Feedstuffs without Clean-Up Step by High-Performance Liquid Chromatography. *Int J Anal Chem, 2018*, 4650764. https://doi.org/10.1155/2018/4650764.

Di Nardo, F., Cavalera, S., Baggiani, C., Giovannoli, C., & Anfossi, L. (2019). Direct vs Mediated Coupling of Antibodies to Gold Nanoparticles: The Case of Salivary Cortisol Detection by Lateral Flow Immunoassay. *ACS Appl Mater Interfaces, 11*(36), 32758-32768. https://doi.org/10.1021/acsami.9b11559.

Flores-Flores, M. E., & Gonzalez-Penas, E. (2017). An LC-MS/MS method for multi-mycotoxin quantification in cow milk. *Food Chem, 218*, 378-385. https://doi.org/10.1016/j.foodchem.2016.09.101.

Gillibert, R., Huang, J. Q., Zhang, Y., Fu, W. L., & Lamy de la Chapelle, M. (2018). Food quality control by Surface Enhanced Raman Scattering. *TrAC Trends in Analytical Chemistry, 105*, 185-190.

https://doi.org/10.1016/j.trac.2018.05.009.

Guo, L., Shao, Y., Duan, H., Ma, W., Leng, Y., Huang, X., & Xiong, Y. (2019). Magnetic Quantum Dot Nanobead-Based Fluorescent Immunochromatographic Assay for the Highly Sensitive Detection of Aflatoxin B_1 in Dark Soy Sauce. *Anal Chem, 91*(7), 4727-4734. https://doi.org/10.1021/acs.analchem.9b00223.

Gurav, R., Surve, S. K., Babar, S., Choudhari, P., Patil, D., More, V., . . . Hangirgekar, S. (2020). Rust-derived Fe_2O_3 nanoparticles as a green catalyst for the one-pot synthesis of hydrazinyl thiazole derivatives. *Org Biomol Chem, 18*(24), 4575-4582. https://doi.org/10.1039/d0ob00109k.

Haque, M. A., Wang, Y., Shen, Z., Li, X., Saleemi, M. K., & He, C. (2020). Mycotoxin contamination and control strategy in human, domestic animal and poultry: A review. *Microb Pathog, 142*, 104095. https://doi.org/10.1016/j.micpath.2020.104095.

Jana, T. K., Pal, A., Mandal, A. K., Sarwar, S., Chakrabarti, P., & Chatterjee, K. (2017). Photocatalytic and Antibacterial Performance of α-Fe_2O_3 Nanostructures. *ChemistrySelect, 2*(10), 3068-3077. https://doi.org/10.1002/slct.201700294.

Jeong, S., Park, J. Y., Cha, M. G., Chang, H., Kim, Y. I., Kim, H. M., . . . Jeong, D. H. (2017). Highly robust and optimized conjugation of antibodies to nanoparticles using quantitatively validated protocols.

Nanoscale, 9(7), 2548-2555. https://doi.org/10.1039/c6nr04683e.

Jia, Y., Zhou, G., Wang, X., Zhang, Y., Li, Z., Liu, P., . . . Zhang, J. (2020). A metal-organic framework/aptamer system as a fluorescent biosensor for determination of aflatoxin B_1 in food samples. *Talanta, 219*, 121342. https://doi.org/10.1016/j.talanta.2020.121342.

Kaspar, P., Sobola, D., Dallaev, R., Ramazanov, S., Nebojsa, A., Rezaee, S., & Grmela, L. (2019). Characterization of Fe_2O_3 thin film on highly oriented pyrolytic graphite by AFM, Ellipsometry and XPS. *Applied Surface Science, 493*, 673-678. https://doi.org/10.1016/j.apsusc.2019.07.058.

Li, Y., Chen, Q., Xu, X., Jin, Y., Wang, Y., Zhang, L., . . . Chen, Y. (2018). Microarray surface enhanced Raman scattering based immunosensor for multiplexing detection of mycotoxin in foodstuff. *Sensors and Actuators B: Chemical, 266*, 115-123. https://doi.org/10.1016/j.snb.2018.03.040.

Lin, S., Liu, X., Tan, L., Cui, Z., Yang, X., Yeung, K. W. K., . . . Wu, S. (2017). Porous Iron-Carboxylate Metal-Organic Framework: A Novel Bioplatform with Sustained Antibacterial Efficacy and Nontoxicity. *ACS Appl Mater Interfaces, 9*(22), 19248-19257. https://doi.org/10.1021/acsami.7b04810.

Liu, S., Dou, L., Yao, X., Zhang, W., Zhao, B., Wang, Z., . . . Wang, J. (2020). Polydopamine nanospheres as high-affinity signal tag

towards lateral flow immunoassay for sensitive furazolidone detection. *Food Chem, 315*, 126310. https://doi.org/10.1016/j.foodchem.2020.126310.

Lou, D., Fan, L., Cui, Y., Zhu, Y., Gu, N., & Zhang, Y. (2018). Fluorescent Nanoprobes with Oriented Modified Antibodies to Improve Lateral Flow Immunoassay of Cardiac Troponin I. *Anal Chem, 90*(11), 6502-6508. https://doi.org/10.1021/acs.analchem.7b05410.

Oplatowska-Stachowiak, M., Sajic, N., Xu, Y., Haughey, S. A., Mooney, M. H., Gong, Y. Y., . . . Elliott, C. T. (2016). Fast and sensitive aflatoxin B_1 and total aflatoxins ELISAs for analysis of peanuts, maize and feed ingredients. *Food Control, 63*, 239-245. https://doi.org/10.1016/j.foodcont.2015.11.041.

Ouyang, J., Zhao, Z., Suib, S. L., & Yang, H. (2019). Degradation of Congo Red dye by a Fe_2O_3@CeO_2-ZrO_2/Palygorskite composite catalyst: Synergetic effects of Fe2O3. *J Colloid Interface Sci, 539*, 135-145. https://doi.org/10.1016/j.jcis.2018.12.052.

Pauly, N., Yubero, F., Espinós, J. P., & Tougaard, S. (2019). XPS primary excitation spectra of Zn 2p, Fe 2p, and Ce 3d from ZnO, α-Fe_2O_3, and CeO_2. *Surface and Interface Analysis, 51*(3), 353-360. https://doi.org/10.1002/sia.6587.

Radu, T., Iacovita, C., Benea, D., & Turcu, R. (2017). X-Ray Photoelectron Spectroscopic Characterization of Iron Oxide Nanoparticles.

Applied Surface Science, 405, 337-343. https://doi.org/10.1016/j.apsusc.2017.02.002.

Rushing, B. R., & Selim, M. I. (2019). Aflatoxin B_1: A review on metabolism, toxicity, occurrence in food, occupational exposure, and detoxification methods. *Food Chem Toxicol, 124*, 81-100. https://doi.org/10.1016/j.fct.2018.11.047.

Schlegel, K. M., & Elsinghorst, P. W. (2020). Myco-DES: Enabling Remote Extraction of Mycotoxins for Robust and Reliable Quantification by Stable Isotope Dilution LC–MS/MS. *Analytical Chemistry, 92*(7), 5387-5395. https://doi.org/10.1021/acs.analchem.0c00087.

Singh, N., Huang, L., Wang, D. B., Shao, N., & Zhang, X. E. (2020). Simultaneous Detection of a Cluster of Differentiation Markers on Leukemia-Derived Exosomes by Multiplex Immuno-Polymerase Chain Reaction via Capillary Electrophoresis Analysis. *Anal Chem, 92*(15), 10569-10577. https://doi.org/10.1021/acs.analchem.0c01464.

Wang, Q., Yang, Q., & Wu, W. (2020). Progress on Structured Biosensors for Monitoring Aflatoxin B_1 From Biofilms: A Review. *Front Microbiol, 11*, 408. https://doi.org/10.3389/fmicb.2020.00408.

Xu, S., Zhang, G., Fang, B., Xiong, Q., Duan, H., & Lai, W. (2019). Lateral Flow Immunoassay Based on Polydopamine-Coated Gold

Nanoparticles for the Sensitive Detection of Zearalenone in Maize. *ACS Appl Mater Interfaces, 11*(34), 31283-31290. https://doi.org/10.1021/acsami.9b08789.

Xu, Z., Long, L.-l., Chen, Y.-q., Chen, M.-L., & Cheng, Y.-H. (2021). A nanozyme-linked immunosorbent assay based on metal–organic frameworks (MOFs) for sensitive detection of aflatoxin B_1. *Food Chemistry, 338*(2021), 128039. https://doi.org/10.1016/j.foodchem.2020.128039.

Yao, X., Wang, Z., Dou, L., Zhao, B., He, Y., Wang, J., . . . Zhang, D. (2019). An innovative immunochromatography assay for highly sensitive detection of 17β-estradiol based on an indirect probe strategy. *Sensors and Actuators B: Chemical, 289*, 48-55. https://doi.org/10.1016/j.snb.2019.03.078.

Zhou, H., Yuan, C., An, Z., Yang, Y., Xu, K., Yu, T., & Luo, X. (2018). Strain-induced phase-structure of Fe_2O_3 nanoparticles. *Journal of Alloys and Compounds, 742*, 7-12. https://doi.org/10.1016/j.jallcom.2018.01.286.

Well-orientation strategy for direct binding of antibodies: Development of the immunochromatographic test using the antigen modified Fe_2O_3 nanoprobes for sensitive detection of aflatoxin B_1

Kunyi He,[†,#] Tong Bu,[†,#] Shuang Zhao,[†] Feier Bai,[†] Meng Zhang,[†] Yongming Tian,[†] Xinyu Sun,[†] Mengna Dong,[†] and Li Wang[†*]

[†] College of Food Science and Engineering, Northwest A&F University, Yangling 712100, Shaanxi, China

[*] Author for correspondence

Tel.: +86 29-8709-2486

Fax: +86 29-8709-2486

lwang@nwsuaf.edu.cn

[#] These authors contributed equally to this work.

ABSTRACT

One of the major concerns in the application of nanocarriers in biosensing is the impair of the recognition molecules bioactivity loaded on their surfaces due to harsh and laborious cross-linking and random orientation, resulting in unsatisfactory sensitivity. Herein, we proposed a novel immunochromatographic test strip (FNS-ag-DICTS) by taking advantage of the antigen (ag) modified Fe_2O_3 nanostructures (FNSs) as new signal tags and goat anti-mouse IgG labeling on the detection line instead of ag,

which was used for sensitive detection of aflatoxin B_1 (AFB_1). The fabricated FNS-ag can orientate the Fab region of monoclonal antibodies (mAbs), waiving the intrinsic limitations of traditional nanomaterials labeled mAbs. Under optimal conditions, FNS-ag-DICTS possessed excellent specificity and a wide detection range, with a visual limit of detection (vLOD) of 0.0125 ng mL^{-1}. In addition, the biosensor successfully detected AFB_1 in peanut, green bean and corn, with an average recovery rate of 82.8-124.9%.

Keywords: Immunochromatographic test strip; Fe_2O_3 nanostructure; Orientated connection; Aflatoxins B_1; High sensitivity

5. Introduction

Because of the simplicity, speed, accuracy, portability and low cost (Aoyama, Monden, Akiyama, Yamada, & Seki, 2019; Guo et al., 2019), immunochromatographic test strips (ICTSs) have evolved into routine techniques in various areas including vitro diagnostics (Xu et al., 2019), environmental monitoring (Di Nardo, Cavalera, Baggiani, Giovannoli, & Anfossi, 2019) and food safety (Zhu et al., 2018), especially the point-of-care testing (POCT) (Di Nardo et al., 2019). However, the conventional gold nanoparticle (AuNPs)-based ICTSs are susceptible to poor performances resulted from small size and low intensity of AuNPs (Huang, Sun, Pu, & Wei, 2019). Nowadays, enormous efforts have been forced on improving sensitivity of ICTS by developing new types of carriers such as rhombic-like Al fluorescent nanosupporter (RlANS) (Bai et al., 2020), silanized Luminescent Quantum Dots (QD-SiO_2) (Goryacheva et al., 2020), bifunctional magnetic fluorescent beads (MFBs) (Guo et al., 2019), two-dimensional

(2D) Pt-Ni$(OH)_2$ nanosheets (NSs) (Cheng et al., 2019), manganese dioxide photothermal nano-carrier (FMD-G NC) (Zhang et al., 2020), etc. Nevertheless, the applicability of these carriers was utterly hampered by complex synthesis process, surface modification, chemical instability, or cumbersome cross-linking with monoclonal antibodies (mAbs) (Lou et al., 2018). In addition, the above methods all made the orientation of the mAbs on the nanomaterials surface random, rendering the Fab region partially or completely losing its access to antigen (ag) (Di Nardo et al., 2019; Lou et al., 2018).

Another direction for improving the performance of ICTS is to strength the bioactivity of mAbs by ameliorating the mAbs' immobilization. For example, Di Nardo et al. proposed to use protein A with biological affinity for mAbs to target specific sites in the Fc region of mAbs (Di Nardo et al., 2019), which can completely expose the Fab region of the mAbs without pre-processing the mAbs, and perfectly retain the antigen binding activity. In addition, Arunas Ramanavicius et al. studied the use of the reducing agent 2-mercaptoethylamine (2-MEA) (Kausaite-Minkstimiene, Ramanavicius, Ruksnaite, & Ramanaviciene, 2013) or dithiothreitol (J. Baniukevic et al., 2013) to split the intact antibody into two half-length fragments (frag-anti) (Makaraviciute, Ruzgas, Ramanavicius, & Ramanaviciene, 2014), and then chemically adsorbed the frag-anti directed fixation for immunoassay (Julija Baniukevic, Kirlyte, Ramanavicius, & Ramanaviciene, 2013). These methods also maximized the binding ability of the probe to the target while retaining the activity of the target binding site (A. Kausaite-Minkstimiene, A. Ramanaviciene, J. Kirlyte, & Ramanavicius, 2010; Zigmas

Balevicius et al., 2011). Unfortunately, the application of free mAbs in biosensing was largely neglected. In fact, compared with mAbs immobilized on the surface of nanomaterials, free specific mAbs featured higher biological activity, faster Brownian motion and more opportunities to bind to the analyte in the sample solution (Butler, Pearce, Nail, Vincent, & Sava Gallis, 2020; Jeong et al., 2017).

Mycotoxins are secondary toxic products of some fungal metabolism (Myndrul et al., 2018; Viter et al., 2018). Among them, aflatoxin B_1 (AFB_1), a bifuran ring toxoid commonly found in grains, oils and their products (Myndrul et al., 2017), is produced mainly by strains such as *Aspergillus flavus* and *Aspergillus parasiticus* (Rushing & Selim, 2019). AFB_1 possesses high toxicity, mutagenicity and carcinogenicity, and it is difficult to degrade, causing AFB_1 to pose a danger to humans and animals (Al-Jaal, Jaganjac, Barcaru, Horvatovich, & Latiff, 2019; Rushing et al., 2019). Due to increasing concerns over food safety and health, it is urgent to establish a sensitive, specific, rapid, and convenient technology for AFB_1 detection.

The Fe_2O_3 nanostructures (FNSs) have gained considerable attention as promising and novel vehicles for various applications due to their high porosity, large surface area, excellent optical property, and chemical stability, which were greatly suitable for labeling protein by general electrostatic adsorption (Bezverkhyy, Popova, Geoffroy, Herbst, & Bellat, 2016; Gurav et al., 2020). In this work, a novel carrier, ag labeled Fe_2O_3 (FNS-ag), with superb optical property and the ability to specifically bind to the Fab fragment domain of mAbs, was synthesized through facile one-step hydrothermal method and applied in the ICTS to sensitively detect the low-level AFB_1 in foods. The

FNS-ag probes could orientate the Fab region of the free mAbs and reduce the amount of mAbs used (Yao et al., 2019). Introducing this probe for ICTS (FNS-ag-DICTS), the competition between free AFB_1 in the sample solution and the fixed ag became more intense due to the significant reduction in the number of free mAbs (Butler et al., 2020; Yao et al., 2019), thereby amplifying the detection signal and helping to improve the sensitivity of the assay. Moreover, the feasibility and applicability of FNS-ag-DICTS was further evaluated by testing AFB_1 in peanut, green bean and corn samples.

6. Materials and methods

2.7 Materials.

Iron chloride hexahydrate ($FeCl_3 \cdot 6H_2O$) was obtained from Guangdong Guanghua Sci-Tech Co., Ltd. (Guangdong, China). N, N'-dimethylformamide (DMF), benzoic acid and methanol were purchased from Chengdu Kelong Chemical Co., Ltd. (Chengdu, China). Bovine serum albumin (BSA) was provided by DIYI Biotechnology Co., Ltd. (Shanghai, China). Goat anti-mouse immunoglobulin (IgG) and anti-AFB_1 monoclonal antibodies (anti-AFB_1 mAbs) were purchased from Wuhan Amyjet Scientific Co., Ltd. (Wuhan, China). Aflatoxin B_1 (AFB_1), aflatoxin B_2 (AFB_2), aflatoxin G_1 (AFG_1), deoxynivalenol (DON), fumonisin B_1 (FB_1), ochratoxin A (OTA), patulin (PAT) and zearalenone (ZEA) (Their chemical structures were shown in Fig. S1) were all offered from Beijing Prime Bio Tek Technology Co., Ltd. (Beijing, China). Nitrocellulose (NC) membrane, glass fiber membrane, polyvinyl chloride plate and absorbent pad were obtained from Shanghai Dening Technology Co., Ltd. (Shanghai, China). Ultrapure water came from the Millipore Milli-Q purification system in our laboratory. Peanut,

green bean and corn samples were all bought from a local supermarket (Yangling, China). All solvents and other chemical reagents used in this experiment were of analytical grade.

2.8 FNSs preparation.

FNSs were first synthesized from $FeCl_3 \cdot 6H_2O$ (99%), benzoic acid (97%), and DMF (99%) with a molar ratio of 1:1:380 by one-step hydrothermal method. After stirring for 15 min, the above solution was mixed in a steel autoclave lined with Teflon, and further heated at 160°C for 72 h. After the solution was cooled down to room temperature, the resulting sediment was collected by centrifugation and washed with DMF 3 times. Ultimately, the synthetic granule product was placed under vacuum and desiccated at 60°C overnight, and stored in a drying cabinet for further use.

2.9 Construction of the directional FNS-ag probes.

Applying a different coupling reaction from the past, directional FNS-ag probes were synthesized innovatively. In short, 1 μg of AFB_1-BSA was added to 1 mL of prepared FNSs solution, and then violently mixed for 40 min at room temperature. The residual binding sites on the surface of FNSs were blocked with 10% BSA solution. The mixture was incubated for 50 min, and the excess reagents were discarded after centrifugation (8300 ×g, 10 min). Finally, the obtained FNS-ag probes were resuspended in 20 μL of ultrapure water and stored at 4°C to conserve biological activity for further use.

2.10 Fabrication of the FNS-ag-DICTS.

In the fabrication of FNS-ag-DICTS, the polyvinyl chloride plate served as the support, onto which the sample pad, conjugate pad, NC membrane and absorption pad

were laminated at an overlapping position of 1-3 mm. The sample and conjugate pads were blocked by immersing in 10 mM phosphate buffered saline (PBS) containing 2% BSA, and then dried at 37°C for 8 h. The test line (T-line) of the NC membrane was painted in IgG (0.5 mg mL^{-1}) at a speed of 0.8 μL cm^{-1}, then the NC membrane was stored at room temperature for drying overnight (Bu et al., 2020; Bu et al., 2019). Finally, all the components were pasted on the plate successively, cut into 3 mm wide strips and stored at 4°C for further use.

2.11 Immunoassay program and performance assessment of FNS-ag-DICTS.

In order to analyze the peculiarity of this FNS-ag-DICTS under the best conditions, different concentrations of AFB_1 were dissolved in the 0.01 M PBS solution to acquire the test samples (0, 0.0064, 0.0125, 0.025, 0.05, 0.1, 0.2, 0.4, 0.8, 1.6, 3.2, 6.4, 12.8, 25.6 ng mL^{-1}). Firstly, 0.4 μL mAbs (0.1 mg mL^{-1}) was incubated with 100 μL test sample solution at room temperature for 20 min, then FNS-ag probes (2.0 μL) were added and mixed. After immersing the sample pad in the above compound for 15 min, the results were recorded by a camera and the T-line signal values were read by a strip reader.

The specificity of the strip was verified by testing AFB_1 (12 ng mL^{-1}) and other mycotoxins including AFB_2, AFG_1, DON, FB_1 OTA, PAT and ZEA (100 ng mL^{-1}).

2.12 Detection of AFB_1 in spiked real samples.

Peanut, green bean and corn were used as real samples in this experiment. The homogeneous foodstuffs (2 g) were triturated, blended severely with 4 mL methanol-PBS (70:30, v/v) for 20 min, and extracted with ultrasonic for 10 min, respectively (Bu

et al., 2019). Then the insoluble matter was removed through centrifugation at 5300 ×g for 10 min. And the obtained supernatant was diluted 10-folds with PBS (0.01 M, pH 7.0). The spiked real samples were analyzed via the prepared FNS-ag-DICTS on the basis of section 2.5.

7. Results and discussions

7.1 Principle of the FNS-ag probes on the emulative FNS-ag-DICTS.

Different from the traditional nanomaterials labeled mAbs as probe, in this paper, the FNSs with excellent water-dispersibility and stability were prepared by one-step hydrothermal method, and AFB_1-BSA could be labeled on their surfaces to form FNS-ag probes (Scheme 1A). For competitive immunoassays, AFB_1-BSA and AFB_1 competed to bind Fab regions of mAbs. In the traditional ICTS, the random combination of nanomaterials and mAbs made some Fab regions of the mAbs blocked, resulting in mAbs unable to effectively participate in the competitive immune response, which greatly limited the sensitivity of detection and wasted mAbs. In the FNS-ag-DICTS strategy, the AFB_1-BSA was preferentially immobilized on the surfaces of the FNSs, the specific binding sites of the Fab regions were not masked because the mAbs were free, which could efficiently bind AFB_1 or FNS-ag probes (Scheme 1B).

In the detection process, the sample solution was mixed with anti-AFB_1 mAbs and incubated for a period of time to make them fully bound, then added the FNS-ag probes to bind the remaining unbound mAbs. The mixture was added to the sample pad, migrated along the sample pad to the absorption pad under the capillary action. If there were no AFB_1 molecules in the sample solution, the FNS-ag-mAb was combined with

the immobilized goat anti-mouse IgG and a visible signal could be discovered on T-line. When AFB_1 existed in the sample, the limited mAbs would bind to AFB_1 firstly, and the remaining mAbs would combine to the FNS-ag probes, so the signal on the T-line would be weaker than the blank. In this measurement mode, the intensity of the color signal was inversely proportional to the concentration of the target in the natural samples. When the concentration of target was high enough, no obvious band can be seen on the T-line (Scheme 1C). In short, the use of FNS-ag probes oriented to connect mAbs effectively reduced the amounts of mAbs, exposed the Fab binding regions of mAbs, and obtained a wide detection range.

3.6 Characterizations of the FNSs and the FNS-ag probes.

As mentioned above, the as-synthesized FNSs were utilized to label AFB_1-BSA as the signal-generation tags in the ICTS. Scanning electron microscopy (SEM) image showed that the prepared FNSs had a cubic shape and were relatively uniformly distributed (Fig. 1A), with an average particle size of 79.53 nm (Fig. 1B). The X-ray diffraction (XRD) pattern of the prepared FNSs matched well with that of standard pattern No.33-0664 in the JCPDS card, proving the formation of Fe_2O_3 (Fig. 1C) (Radu, Iacovita, Benea, & Turcu, 2017). To confirm the successful preparation of FNSs, X-ray photoelectron spectroscopy (XPS) was used for analysis. Fig. 1D indicated that the synthesized FNSs mainly composed of three elements Fe, O and C. The two peaks worthy of consideration were located at around 710 eV and 724 eV, which belonged to Fe $2p_{1/2}$ and Fe $2p_{3/2}$, respectively. The peaks at 719 eV and 733 eV were the satellite peaks of Fe^{3+}, which were exactly the same as the characteristic peaks of Fe_2O_3

nanoparticles (Fig. 1E) (Abhilash, Gangadhar, Krishnegowda, Chikkamadaiah, & Srikantaswamy, 2019; Gurav et al., 2020; Pauly, Yubero, Espinós, & Tougaard, 2019). Further analysis of the fitted O 1s spectrum (Figure 1F) showed that the main O 1s peak occurred at 530.25 eV, which was ascribed to Ox^{2-}, confirming the presence of Fe_2O_3 compound. The subpeaks at 531.5 eV and 532.8 eV were commonly attributed to OH^- and O_2^{2-} / O^-, respectively (Kaspar et al., 2019).

Moreover, UV-vis spectroscopy confirmed that FNSs can bind to protein (Fig. 1G). The characteristic absorption peak of BSA was observed in the FNS-BSA at 280 nm, demonstrating that the protein was successfully labeled upon the surface of FNSs. Fourier transform infrared (FT-IR) spectroscopy was scanned to ascertain the composition of FNSs. The characteristic absorption signals of Fe-O bond appeared around at 565 cm^{-1}, and the signals at near 3466 cm^{-1} and 1634 cm^{-1} were identified as -OH and C=O stretching vibration and bending vibration, respectively (Jana et al., 2017; Ouyang, Zhao, Suib, & Yang, 2019; Zhou et al., 2018). In addition, the FT-IR spectrum of FNS-BSA had the same characteristic absorption peaks as those of FNSs and BSA (Fig. 1H), indicating that protein was indeed connected to FNSs (Cheng et al., 2019). To further evaluate that FNSs can label protein, sodium dodecyl sulfate-polyacrylamide gel electrophoresis (SDS-PAGE) was used for analysis. In Fig. 1I, there was no band when only FNSs were presented, while both of BSA and FNS-BSA had blue bands at a molecular weight of about 60 kDa, which proved that FNSs can couple protein well (Bu et al., 2020).

3.7 Optimization of Analytical conditions.

In this work, the signal intensity on the T-lines (FI_T) for the AFB_1-free sample and the competitive inhibition rate for the AFB_1-spiked sample (12.8 ng mL^{-1}) were adopted to select the optimal detection parameters. The competitive inhibition rate was calculated by $(1-B/B_0) \times 100\%$, where B_0 and B were FI_T values of AFB_1-free and AFB_1-spiked solutions, respectively. The optimization results of the key parameters were shown in the supplementary materials. In summary, the optimal amount of AFB_1-BSA was selected as 10 μg mL^{-1}, the concentration of IgG was 0.5 mg mL^{-1} on T-line, the optimal volume of FNS-ag probe was 2 μL, the optimal dosage of anti-AFB_1 mAbs was 0.4 μg mL^{-1}, 20 min was selected as the best incubation time of AFB_1 and mAbs, 15 min was regarded as the optimal immunoreaction time (Figure 2), the optimal BSA closure time was 50 min and the optimal reaction pH was 7 (Figure S2).

3.4 Analytical performance of FNS-ag-DICTS.

Sensitivity is an essential parameter to evaluate the performance of FNS-ag-DICTS. Under the optimized conditions, a series of concentrations of AFB_1 standard solutions were tested to evaluate the sensitivity and dynamic range of the proposed platform. The result in Fig. 3A showed that the color intensity of the T-line decreased with the concentration of AFB_1 increased. In addition, when the concentration of AFB_1 was 0.0125 ng mL^{-1}, the T-line intensity was different from that of the negative control strip. Here, 0.0125 ng mL^{-1} could be regarded as the visual detection limit (vLOD) (The vLOD was defined as the lowest concentration of the target whose observed T-line color was weaker than that of the blank) of the FNS-ag-DICTS.

In this study, the standard curve of the FNS-ag-DICTS for AFB_1 quantitative

determination was indicated by drawing the intensity value of T-line vs the logarithm of AFB_1 concentrations (0-25.6 ng mL^{-1}). The standard curve exhibited a good linear relationship in the detection range of AFB_1 from 0 to 12.8 ng mL^{-1}, the correlation coefficient R^2=0.994, the IC_{50} value of FNS-ag-DICTS was 0.30 ng mL^{-1}, and the regression equation could be expressed as Y= -226.44X+346.48, where X and Y were represented Lg [AFB_1 concentration] and T-line intensity, respectively (Fig. 3B).

The selectivity of the FNS-ag-DICTS was evaluated by analyzing two common structural analogues AFB_2 and AFG_1 (100 ng mL^{-1}) and five other common mycotoxins (DON, FB_1, OTA, PAT, ZEA) (100 ng mL^{-1}). In Fig. 3C and 3D, the developed FNS-ag-DICTS only exhibited a lighter T-line color in the presence of AFB_2 and AFG_1, while the T-line intensities of other mycotoxins were basically the same as the negative control strip. In order to further confirm the specificity of FNS-ag-DICTS, the same anti-AFB_1 mAbs were also used to detect 12.8 ng mL^{-1} of AFB_1 and 100 ng mL^{-1} of other toxins by competitive ELISA (Fig. S5). The results indicated that except for AFB_2 and AFG_1 (less than 0.1), the values of other toxins were the same as the control (about equal to 1). The above results demonstrated that the prepared FNS-ag-DICTS had high specificity for the detection of AFB_1.

3.5 Performance comparison of FNS-ag-DICTS and FNS-mAb-ICTS

To confirm the improvement of sensor sensitivity, the performance of traditional FNS-mAb-ICTS was tested. As shown in Fig. S4, the vLOD of AFB_1 detected by traditional FNS-mAb-ICTS was 0.09 ng mL^{-1}. Thus, the sensitivity of the developed FNS-ag-DICTS using FNS-ag as a probe was at least seven times higher than that of

traditional FNS-mAb-ICTS. This fact may be because the amount of mAb used in FNS-ag-DICTS was less than that of FNS-mAb-ICTS, which improved the sensitivity (Tong Bu et al., 2020; Liu et al., 2020; Yao et al., 2019). In addition, the vLOD of FNS-ag-DICTS was lower than most previous reports on the detection of AFB_1 (Table S1).

Furthermore, FNS indicated 93.2% of coupling efficiency at the mAbs concentration of 10 μg mL^{-1} (Fig. S6), which was significantly lower than 100% utilization rate of the free mAbs in FNS-ag-DICTS. In order to illustrate that the free mAbs with directional binding had better target affinity than the immobilized mAbs on FNS, the affinity constant *K*a of the mAbs was estimated according to a four-parameter logistic regression model (Fig. S7) and the following formula:

$$Ka=(n-1)/2(n[Ab]_1-[Ab]_2) \quad (1)$$

Where $[Ab]_1$ and $[Ab]_2$ correspond to the antibody molar concentration of the two coating concentrations at their respective ODmax/2 absorbance values, n refers to the ratio of the two coating concentrations (n>1).

The higher *K*a indicates the higher the binding affinity of the antigen and antibody (Lee et al., 2014; Peltomaa et al., 2020). The *K*a values of free mAbs and FNS-mAb were 1.4×10^8 and 8.6×10^7, respectively, indicating that a well-oriented free mAbs possessed stronger antigen affinity than FNS-mAb.

3.6 AFB_1 analysis in actual samples.

In order to further prove the feasibility of the FNS-ag-DICTS in the application of food samples, the peanut, green bean and corn samples were first processed according to the previous method, and then the acquired sample solutions were detected by the

FNS-ag-DICTS. As shown in Fig. 4, as the concentration of AFB_1 increased, the T-line intensity gradually decreased. At the same time, the vLODs of AFB_1 in the three spiked samples were all 0.1 ng g^{-1}. In addition, the results in Table 1 showed that the average recovery rate of AFB_1 was 82.8-124.9%, and the relative standard deviation (RSD) values was lower than 5.9%. The above results showed that the developed FNS-ag-DICTS could be used for AFB_1 detection in complex foods after simple pretreatment, and possessed good application potential and reproducibility.

8. Conclusion

In conclusion, we successfully developed FNS-ag-DICTS for the highly sensitive detection of AFB_1 by using FNS-ag as a probe and labeling the goat anti-mouse IgG on the T-line. The reported FNS-ag probe had a large specific surface area, excellent stability, and directional coupling to free mAbs. This advanced binding method avoided the masking of the mAb's antigen binding site due to the direct coupling of the mAbs to the nanomaterials, thus reducing the amount of mAbs and effectively improving the sensitivity. Under optimal conditions, the detection limit of novel FNS-ag-DICTS was 0.0125 ng mL^{-1}, which was 7 times lower than the traditional FNS-mAb-ICTS (0.09 ng mL^{-1}). In addition, FNS-ag-DICTS had the wide detection range, and excellent specificity and which also can efficiently screen low-leave AFB_1 in peanut, green bean and corn samples. More importantly, the immunoassay strategy of directly coupling mAbs can be flexibly extended to highly sensitive on-site detection of other analytes by easily transforming the type of antigen modified nanomaterials and mAbs.

Declaration of interests

The authors declare no competing financial interest.

Acknowledgments

This work was supported by Talented Program (A279021724) and the Fundamental Research Funds for the Northwest A&F University (Nos. Z111021601).

References

A. Kausaite-Minkstimiene, A. Ramanaviciene, J. Kirlyte, & Ramanavicius, A. (2010). Comparative Study of Random and Oriented Antibody Immobilization Techniques on the Binding Capacity of Immunosensor. *Anal Chem,* 6401-6408. https://doi.org/10.1021/ac100468k.

Abhilash, M. R., Gangadhar, A., Krishnegowda, J., Chikkamadaiah, M., & Srikantaswamy, S. (2019). Hydrothermal synthesis, characterization and enhanced photocatalytic activity and toxicity studies of a rhombohedral Fe_2O_3 nanomaterial. *RSC Advances, 9*(43), 25158-25169. https://doi.org/10.1039/c9ra04978a.

Al-Jaal, B. A., Jaganjac, M., Barcaru, A., Horvatovich, P., & Latiff, A. (2019). Aflatoxin, fumonisin, ochratoxin, zearalenone and deoxynivalenol biomarkers in human biological fluids: A systematic literature review, 2001-2018. *Food Chem Toxicol, 129*, 211-228. https://doi.org/10.1016/j.fct.2019.04.047.

Aoyama, S., Monden, K., Akiyama, Y., Yamada, M., & Seki, M. (2019). Enhanced Immunoadsorption on Imprinted Polymeric Microstructures with Nanoengineered Surface Topography for Lateral Flow Immunoassay Systems. *Anal Chem, 91*(21), 13377-13382. https://doi.org/10.1021/acs.analchem.9b03454.

Bai, F., Bu, T., Zhang, M., Tian, Y., Sun, X., Jia, P., Wang, L. (2020). Rhombic-like Al nanosupporter-based fluorescent immunochromatographic assay for the sensitive detection of tetracycline. *Sensors and Actuators B: Chemical, 324*.

128721. https://doi.org/10.1016/j.snb.2020.128721.

Baniukevic, J., Hakki Boyaci, I., Goktug Bozkurt, A., Tamer, U., Ramanavicius, A., & Ramanaviciene, A. (2013). Magnetic gold nanoparticles in SERS-based sandwich immunoassay for antigen detection by well oriented antibodies. *Biosens Bioelectron, 43*, 281-288. https://doi.org/10.1016/j.bios.2012.12.014.

Baniukevic, J., Kirlyte, J., Ramanavicius, A., & Ramanaviciene, A. (2013). Application of oriented and random antibody immobilization methods in immunosensor design. *Sensors and Actuators B: Chemical, 189*, 217-223. https://doi.org/10.1016/j.snb.2013.03.126.

Bezverkhyy, I., Popova, E., Geoffroy, N., Herbst, F., & Bellat, J. P. (2016). Preparation of magnetic composites of MIL-53(Fe) or MIL-100(Fe) via partial transformation of their framework into γ-Fe_2O_3. *Journal of Materials Chemistry A, 4*(21), 8141-8148. https://doi.org/10.1039/c6ta00383d.

Bu, T., Jia, P., Sun, X., Liu, Y., Wang, Q., & Wang, L. (2020). Hierarchical molybdenum disulfide nanosheets based lateral flow immunoassay for highly sensitive detection of tetracycline in food samples. *Sensors and Actuators B: Chemical, 320*. 128440. https://doi.org/10.1016/j.snb.2020.128440.

Bu, T., Yao, X., Huang, L., Dou, L., Zhao, B., Yang, B., .Zhang, D. (2020). Dual recognition strategy and magnetic enrichment based lateral flow assay toward Salmonella enteritidis detection. *Talanta, 206*, 120204. https://doi.org/10.1016/j.talanta.2019.120204.

Bu, T., Zhang, M., Sun, X., Tian, Y., Bai, F., Jia, P., Wang, L. (2019). Gold

nanoparticles-functionalized microorganisms assisted construction of immunobiosensor for sensitive detection of ochratoxin A in food samples. *Sensors and Actuators B: Chemical, 299*. 126969. https://doi.org/10.1016/j.snb.2019.126969.

Butler, K. S., Pearce, C. J., Nail, E. A., Vincent, G. A., & Sava Gallis, D. F. (2020). Antibody Targeted Metal-Organic Frameworks for Bioimaging Applications. *ACS Appl Mater Interfaces, 12*(28), 31217-31224. https://doi.org/10.1021/acsami.0c07835.

Cheng, N., Shi, Q., Zhu, C., Li, S., Lin, Y., & Du, D. (2019). Pt-Ni$(OH)_2$ nanosheets amplified two-way lateral flow immunoassays with smartphone readout for quantification of pesticides. *Biosens Bioelectron, 142*, 111498. https://doi.org/10.1016/j.bios.2019.111498.

Di Nardo, F., Cavalera, S., Baggiani, C., Giovannoli, C., & Anfossi, L. (2019). Direct vs Mediated Coupling of Antibodies to Gold Nanoparticles: The Case of Salivary Cortisol Detection by Lateral Flow Immunoassay. *ACS Appl Mater Interfaces, 11*(36), 32758-32768. https://doi.org/10.1021/acsami.9b11559.

Goryacheva, O. A., Guhrenz, C., Schneider, K., Beloglazova, N. V., Goryacheva, I. Y., De Saeger, S., & Gaponik, N. (2020). Silanized Luminescent Quantum Dots for the Simultaneous Multicolor Lateral Flow Immunoassay of Two Mycotoxins. *ACS Appl Mater Interfaces, 12*(22), 24575-24584. https://doi.org/10.1021/acsami.0c05099.

Guo, L., Shao, Y., Duan, H., Ma, W., Leng, Y., Huang, X., & Xiong, Y. (2019).

Magnetic Quantum Dot Nanobead-Based Fluorescent Immunochromatographic Assay for the Highly Sensitive Detection of Aflatoxin B_1 in Dark Soy Sauce. *Anal Chem, 91*(7), 4727-4734. https://doi.org/10.1021/acs.analchem.9b00223.

Gurav, R., Surve, S. K., Babar, S., Choudhari, P., Patil, D., More, V., Hangirgekar, S. (2020). Rust-derived Fe_2O_3 nanoparticles as a green catalyst for the one-pot synthesis of hydrazinyl thiazole derivatives. *Org Biomol Chem, 18*(24), 4575-4582. https://doi.org/10.1039/d0ob00109k.

Huang, L., Sun, D. W., Pu, H., & Wei, Q. (2019). Development of Nanozymes for Food Quality and Safety Detection: Principles and Recent Applications. *Compr Rev Food Sci Food Saf, 18*(5), 1496-1513. https://doi.org/10.1111/1541-4337.12485.

Jana, T. K., Pal, A., Mandal, A. K., Sarwar, S., Chakrabarti, P., & Chatterjee, K. (2017). Photocatalytic and Antibacterial Performance of α-Fe_2O_3 Nanostructures. *ChemistrySelect, 2*(10), 3068-3077. https://doi.org/10.1002/slct.201700294.

Jeong, S., Park, J. Y., Cha, M. G., Chang, H., Kim, Y. I., Kim, H. M., Jeong, D. H. (2017). Highly robust and optimized conjugation of antibodies to nanoparticles using quantitatively validated protocols. *Nanoscale, 9*(7), 2548-2555. https://doi.org/10.1039/c6nr04683e.

Kaspar, P., Sobola, D., Dallaev, R., Ramazanov, S., Nebojsa, A., Rezaee, S., & Grmela, L. (2019). Characterization of Fe_2O_3 thin film on highly oriented pyrolytic graphite by AFM, Ellipsometry and XPS. *Applied Surface Science, 493*, 673-678. https://doi.org/10.1016/j.apsusc.2019.07.058.

Kausaite-Minkstimiene, A., Ramanavicius, A., Ruksnaite, J., & Ramanaviciene, A. (2013). A surface plasmon resonance immunosensor for human growth hormone based on fragmented antibodies. *Analytical Methods, 5*(18). 4757. https://doi.org/10.1039/c3ay40614h.

Lee, E. J., Lee, E., Kim, H. J., Lee, J. H., Ahn, K. Y., Park, J. S., & Lee, J. (2014). Self-assembled proteinticle nanostructures for 3-dimensional display of antibodies. *Nanoscale, 6*(24), 14919-14925. https://doi.org/10.1039/c4nr03635b.

Liu, S., Dou, L., Yao, X., Zhang, W., Zhao, B., Wang, Z., Wang, J. (2020). Polydopamine nanospheres as high-affinity signal tag towards lateral flow immunoassay for sensitive furazolidone detection. *Food Chem, 315*, 126310. https://doi.org/10.1016/j.foodchem.2020.126310.

Lou, D., Fan, L., Cui, Y., Zhu, Y., Gu, N., & Zhang, Y. (2018). Fluorescent Nanoprobes with Oriented Modified Antibodies to Improve Lateral Flow Immunoassay of Cardiac Troponin I. *Anal Chem, 90*(11), 6502-6508. https://doi.org/10.1021/acs.analchem.7b05410.

Makaraviciute, A., Ruzgas, T., Ramanavicius, A., & Ramanaviciene, A. (2014). Antibody fragment immobilization on planar gold and gold nanoparticle modified quartz crystal microbalance with dissipation sensor surfaces for immunosensor applications. *Anal. Methods, 6*(7), 2134-2140. https://doi.org/10.1039/c4ay00070f.

Myndrul, V., Viter, R., Savchuk, M., Koval, M., Starodub, N., Silamikelis, V., Iatsunskyi, I. (2017). Gold coated porous silicon nanocomposite as a substrate

for photoluminescence-based immunosensor suitable for the determination of Aflatoxin B_1. *Talanta, 175*, 297-304. https://doi.org/10.1016/j.talanta.2017.07.054.

Myndrul, V., Viter, R., Savchuk, M., Shpyrka, N., Erts, D., Jevdokimovs, D., Iatsunskyi, I. (2018). Porous silicon based photoluminescence immunosensor for rapid and highly-sensitive detection of Ochratoxin A. *Biosens Bioelectron, 102*, 661-667. https://doi.org/10.1016/j.bios.2017.11.048.

Ouyang, J., Zhao, Z., Suib, S. L., & Yang, H. (2019). Degradation of Congo Red dye by a Fe_2O_3@CeO_2-ZrO_2/Palygorskite composite catalyst: Synergetic effects of Fe_2O_3. *J Colloid Interface Sci, 539*, 135-145. https://doi.org/10.1016/j.jcis.2018.12.052.

Pauly, N., Yubero, F., Espinós, J. P., & Tougaard, S. (2019). XPS primary excitation spectra of Zn 2p, Fe 2p, and Ce 3d from ZnO, α-Fe_2O_3, and CeO_2. *Surface and Interface Analysis, 51*(3), 353-360. https://doi.org/10.1002/sia.6587.

Peltomaa, R., Farka, Z., Mickert, M. J., Brandmeier, J. C., Pastucha, M., Hlavacek, A., Gorris, H. H. (2020). Competitive upconversion-linked immunoassay using peptide mimetics for the detection of the mycotoxin zearalenone. *Biosens Bioelectron, 170*, 112683. https://doi.org/10.1016/j.bios.2020.112683.

Radu, T., Iacovita, C., Benea, D., & Turcu, R. (2017). X-Ray Photoelectron Spectroscopic Characterization of Iron Oxide Nanoparticles. *Applied Surface Science, 405*, 337-343. https://doi.org/10.1016/j.apsusc.2017.02.002.

Rushing, B. R., & Selim, M. I. (2019). Aflatoxin B_1: A review on metabolism, toxicity,

occurrence in food, occupational exposure, and detoxification methods. *Food Chem Toxicol, 124*, 81-100. https://doi.org/10.1016/j.fct.2018.11.047.

Viter, R., Savchuk, M., Iatsunskyi, I., Pietralik, Z., Starodub, N., Shpyrka, N., Ramanavicius, A. (2018). Analytical, thermodynamical and kinetic characteristics of photoluminescence immunosensor for the determination of Ochratoxin A. *Biosens Bioelectron, 99*, 237-243. https://doi.org/10.1016/j.bios.2017.07.056.

Xu, S., Zhang, G., Fang, B., Xiong, Q., Duan, H., & Lai, W. (2019). Lateral Flow Immunoassay Based on Polydopamine-Coated Gold Nanoparticles for the Sensitive Detection of Zearalenone in Maize. *ACS Appl Mater Interfaces, 11*(34), 31283-31290. https://doi.org/10.1021/acsami.9b08789.

Yao, X., Wang, Z., Dou, L., Zhao, B., He, Y., Wang, J., Zhang, D. (2019). An innovative immunochromatography assay for highly sensitive detection of 17β-estradiol based on an indirect probe strategy. *Sensors and Actuators B: Chemical, 289*, 48-55. https://doi.org/10.1016/j.snb.2019.03.078.

Zhang, M., Bu, T., Bai, F., Zhao, S., Tian, Y., He, K., Wang, L. (2020). Gold nanoparticles-functionalized three-dimensional flower-like manganese dioxide: A high-sensitivity thermal analysis immunochromatographic sensor. *Food Chem, 341*(Pt 1), 128231. https://doi.org/10.1016/j.foodchem.2020.128231.

Zhou, H., Yuan, C., An, Z., Yang, Y., Xu, K., Yu, T., & Luo, X. (2018). Strain-induced phase-structure of Fe_2O_3 nanoparticles. *Journal of Alloys and Compounds, 742*, 7-12. https://doi.org/10.1016/j.jallcom.2018.01.286.

Zhu, C., Zhang, G., Huang, Y., Yang, S., Ren, S., Gao, Z., & Chen, A. (2018). Dual-competitive lateral flow aptasensor for detection of aflatoxin B_1 in food and feedstuffs. *J Hazard Mater, 344*, 249-257. https://doi.org/10.1016/j.jhazmat.2017.10.026.

Zigmas Balevicius, Almira Ramanaviciene, Ieva Baleviciute, Asta Makaraviciute, Lina Mikoliunaite, & Ramanavicius, A. (2011). Evaluation of intact- and fragmented-antibody based immunosensors by total internal reflection ellipsometry. *Sensors and Actuators B: Chemical*, 555-562. https://doi.org/10.1016/j.snb.2011.08.029.

Credit Author Statement

Kunyi He: Conceptualization, Methodology**,** Formal Analysis, Writing - original draft. **Tong Bu:** Conceptualization, Methodology**,** Formal Analysis, Writing - original draft. **Shuang Zhao:** Validation, Visualization. **Feier Bai:** Validation, Visualization. **Meng Zhang:** Validation, Visualization. **Yongming Tian:** Validation, Visualization. **Xinyu Sun:** Validation, Visualization. **Mengna Dong:** Validation, Visualization. **Li Wang:** Conceptualization, Writing - Review & Editing, Supervision, Project Administration.

Table 1. Recovery rate of AFB_1 spiked in peanut, green bean and corn samples detected by the FNS-ag-DICTS.

Sample	Added (ng mL^{-1})	Found (ng mL^{-1})	Recovery (%)	RSD (%)
	0.125	0.129	103.5	1.4

Peanut	0.05	0.054	107.5	1.9
	0.8	0.988	123.5	2.5
	0.125	0.121	97.1	1.4
Green bean	0.05	0.049	97.7	0.6
	0.8	0.825	103.1	1.2
	0.125	0.103	82.8	0.8
Corn	0.05	0.061	122.1	1.1
	0.8	0.999	124.9	5.9

Highlights

• A sensitive sensor that utilized oriented probe was developed to detect aflatoxin B_1.

• The Fe_2O_3-antigen probe directionally connected antibodies and improved bioactivity.

• The proposed strategy possessed a low detection limit and wide detection range.

• Satisfactory analytical results in real foodstuffs showed the sensor's feasibility.

Declaration of interests

☒ The authors declare that they have no known competing financial interests or personal relationships that could have appeared to influence the work reported in this paper.

☐The authors declare the following financial interests/personal relationships which may be considered as potential competing interests:

Figure Captions

Scheme 1. (A) Scheme for the synthesis of FNS-ag probes; (B) Principle illustration of the detection strategy for traditional FNS-mAb-ICTS; (C) Principle illustration of the detection strategy for AFB_1 by FNS-ag-DICTS.

Fig. 1. Characterizations for the FNSs and FNS-ag probes. (A) SEM image for FNSs; (B) Particle diameter distribution of the FNSs; (C) XRD pattern of FNSs; (D) XPS pattern of the FNSs; High-resolution XPS spectra of (E) Fe 2p, (F) O 1s of the FNSs; (G) UV–vis absorbance spectra of FNSs, BSA and the FNS-ag probes; (H) FT-IR spectra of the FNSs, BSA and the FNS-ag probes; (I) SDS-PAGE image of the FNSs, BSA and FNS-ag probes: Ⅰ, Marker; Ⅱ, FNSs; Ⅲ, BSA; Ⅳ, FNS-ag probes.

Fig. 2. Optimization of the FNS-ag-DICTS. Effects of (A) amount of AFB_1-BSA; (B) amount of goat anti-mouse IgG; (C) volume of FNS-ag probes; (D) amount of anti-AFB_1 mAbs; (E) incubating time of FNS-ag probes and AFB_1; (D) immunoreaction time on the FNS-ag-DICTS.

Fig. 3. Assay performances of the FNS-ag-DICTS for AFB_1 detection. (A) Photographs of the FNS-ag-DICTS for different amounts of AFB_1 (a-n represent 0, 0.006, 0.0125, 0.025, 0.05, 0.1, 0.2, 0.4, 0.8, 1.6, 3.2, 6.4, 12.8, 25.6 ng mL^{-1}, respectively); (B) The change rule of FNS-ag-DICTS in the range of AFB_1 0-25.6 ng mL^{-1}, the illustration

shows the calibration curve; (C) Photographs of specific results of FNS-ag-DICTS detecting AFB_1 and other toxins; (D) The specific results of AFB_1 (12.8 ng mL^{-1}) and 100 ng mL^{-1} other toxins were detected by FNS-ag-DICTS.

Fig. 4. Practicability test of the FNS-ag-DICTS for real sample detection: (A, B) peanut, (C, D) green bean and (E, F) corn. (a-n represent 0, 0.006, 0.0125, 0.025, 0.05, 0.1, 0.2, 0.4, 0.8, 1.6, 3.2, 6.4, 12.8, 25.6 ng g^{-1}, respectively).

Scheme 1

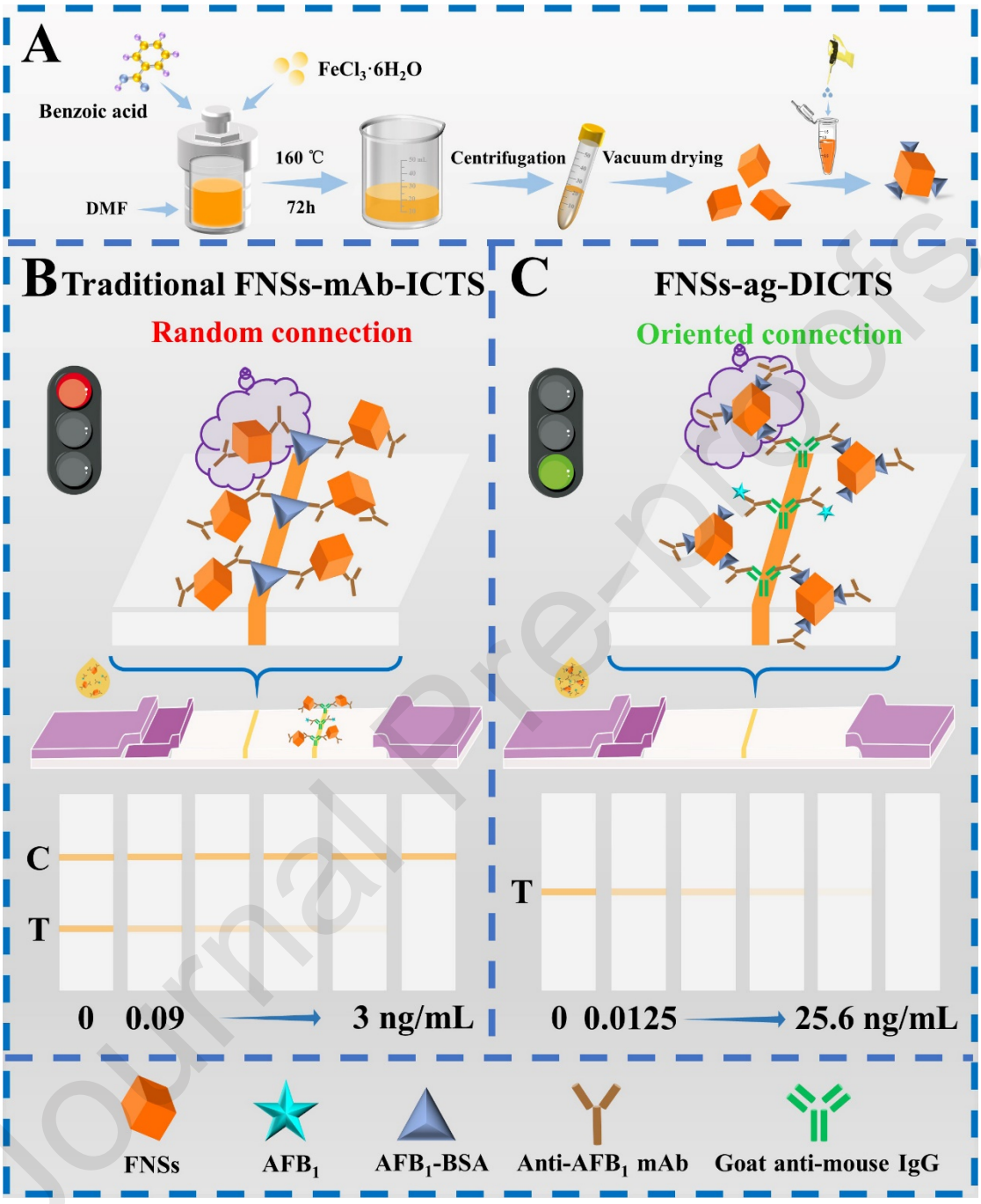

Fig. 1

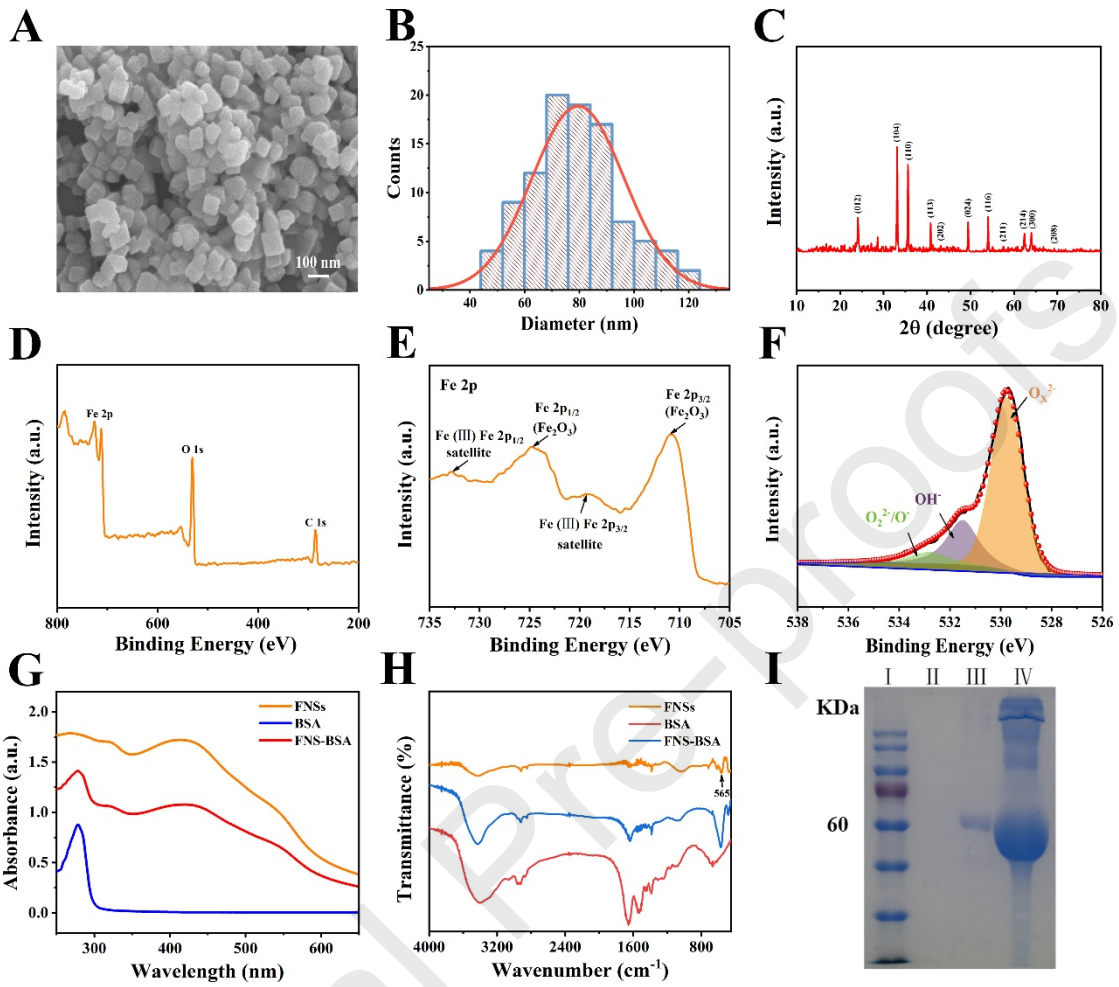

Fig. 2

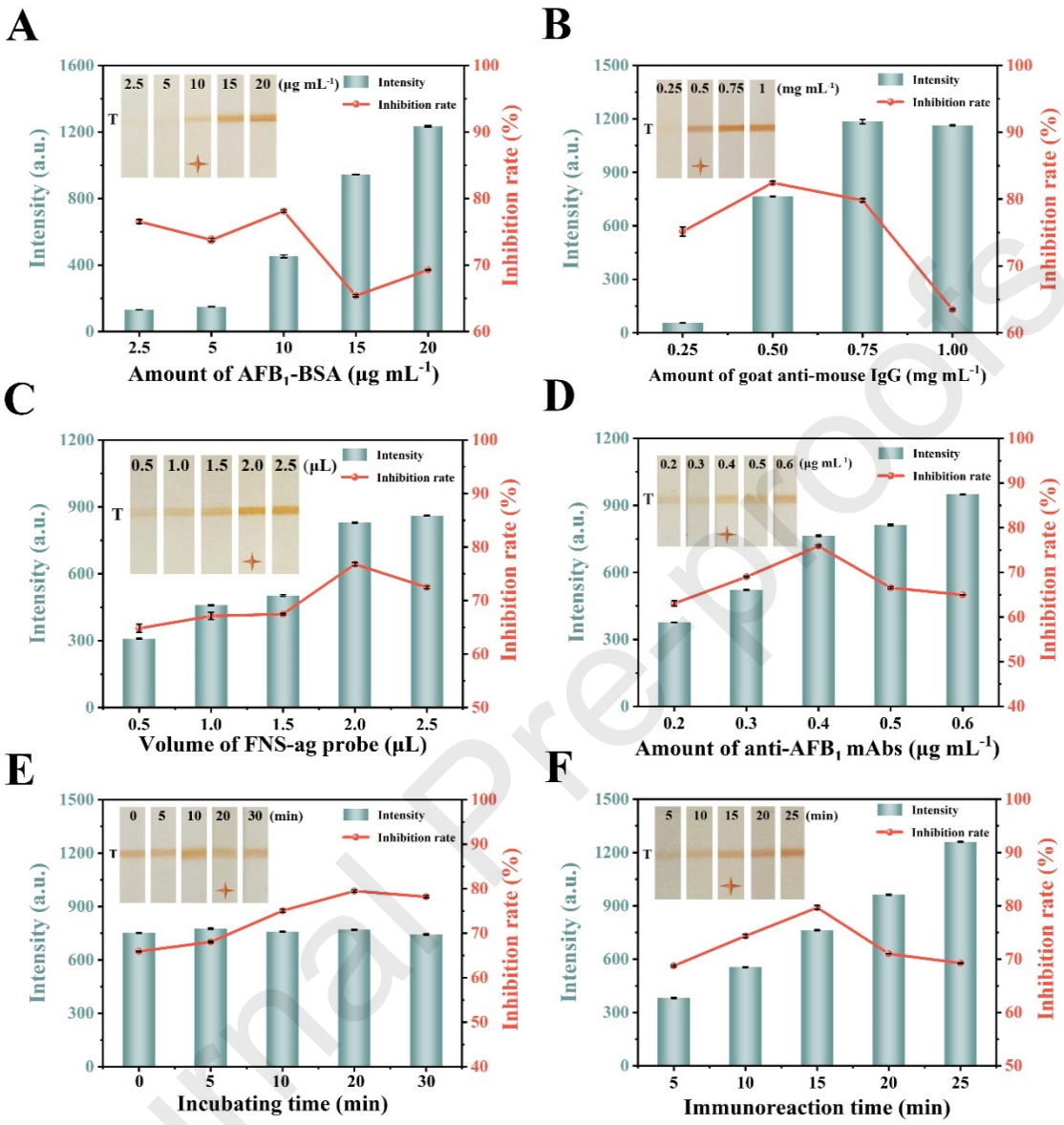

Fig. 3

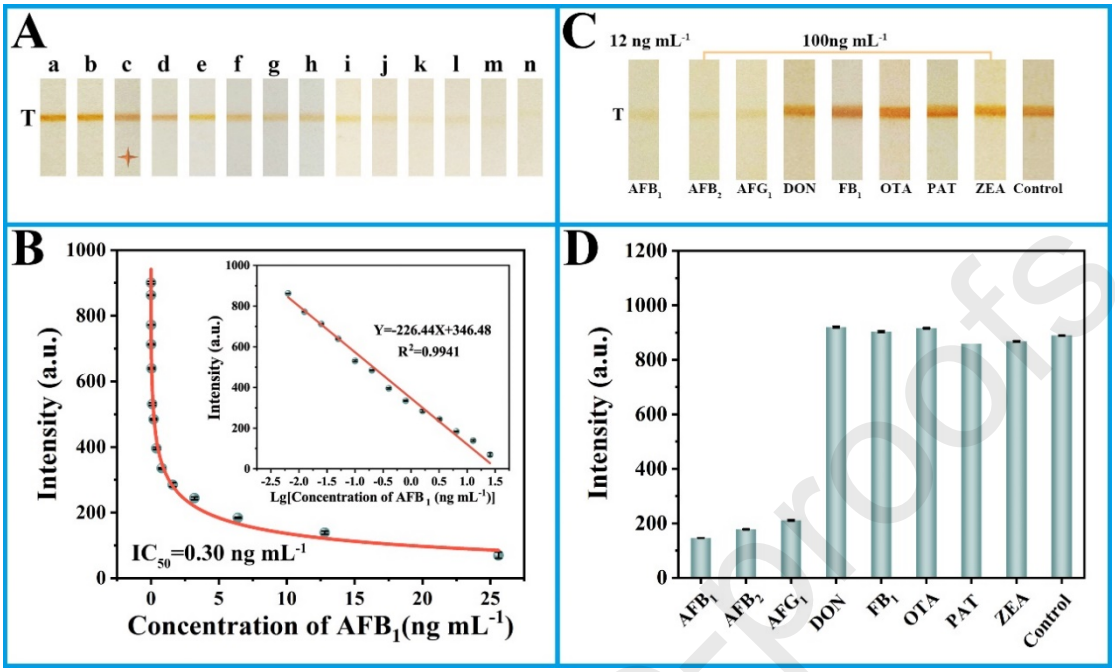
A
a b c d e f g h i j k l m n
T
C
12 ng mL-1
100ng mL-1
T
AFB1 AFB2 AFG1 DON FB1 OTA PAT ZEA Control
B
Intensity (a.u.)
Concentration of AFB1(ng mL-1)
IC50=0.30 ng mL-1
Y=-226.44X+346.48
R2=0.9941
Lg[Concentration of AFB1 (ng mL-1)]
D
Intensity (a.u.)
AFB1 AFB2 AFG1 DON FB1 OTA PAT ZEA Control

Fig. 4